Stem Cell Research & Therapy

RESEARCH

Open Access

Mesenchymal stromal cells alleviate APAP-induced liver injury via extracellular vesicle-mediated regulation of the miR-186-5p/CXCL1 axis

Erming Zhao[1†], Rukang Liang[1†], Panlong Li[1†], Di Lu[1], Shuhan Chen[1], Weikeng Tan[1], Yunfei Qin[1], Yana Zhang[2,3], Yingcai Zhang[4*], Qi Zhang[1*] and Qiuli Liu[1*]

Abstract

Background Acetaminophen (APAP) overdose is a significant cause of drug-induced liver injury (DILI). N-acetylcysteine (NAC) is the first-line agent used in the clinic. However, it rarely benefits patients with advanced APAP toxicity. Mesenchymal stromal cells (MSCs) have demonstrated potential in treating DILI. However, the specific mechanism by which MSCs protect against APAP-induced liver injury remains unclear.

Methods APAP was injected intraperitoneally to induce a liver injury model. We then detected histopathology, biochemical indices, and inflammatory cytokine levels to assess the efficacy of MSCs and MSC extracellular vesicles (MSC-EVs). Flow cytometry was performed to reveal the immunoregulatory effects of MSCs and MSC-EVs on the neutrophils. RNA sequencing (RNA-Seq) of liver tissues was used to identify critical target genes for MSC treatment.

Results MSC and MSC-EV treatment effectively alleviated APAP-induced liver injury and inhibited neutrophil infiltration. RNA-Seq analysis and ELISA data indicated that C-X-C motif chemokine 1 (CXCL1), a chemoattractant for neutrophils, was a key molecule in the MSC-mediated amelioration of APAP-induced liver damage. In addition, neutralization of CXCL1 reduced APAP-induced liver damage, which was accompanied by decreased neutrophil infiltration. Importantly, we verified that MSC-EV-derived miR-186-5p directly binds to the 3′-UTR of Cxcl1 to inhibit its expression in hepatocytes. The agomir miR-186-5p showed excellent potential for the treatment of DILI.

†Erming Zhao, Rukang Liang and Panlong Li contributed equally to this work and share first authorship.

*Correspondence:
Yingcai Zhang
zhangyc3@mail.sysu.edu.cn
Qi Zhang
zhangq27@mail.sysu.edu.cn
Qiuli Liu
liuqli3@mail.sysu.edu.cn

Full list of author information is available at the end of the article

Conclusions Our findings suggest that MSCs and MSC-EVs are an effective approach to mitigate DILI. Targeting the miR-186-5p/CXCL1 axis is a promising approach to improve the efficacy of MSCs and MSC-EVs in the treatment of DILI.

Graphical Abstract

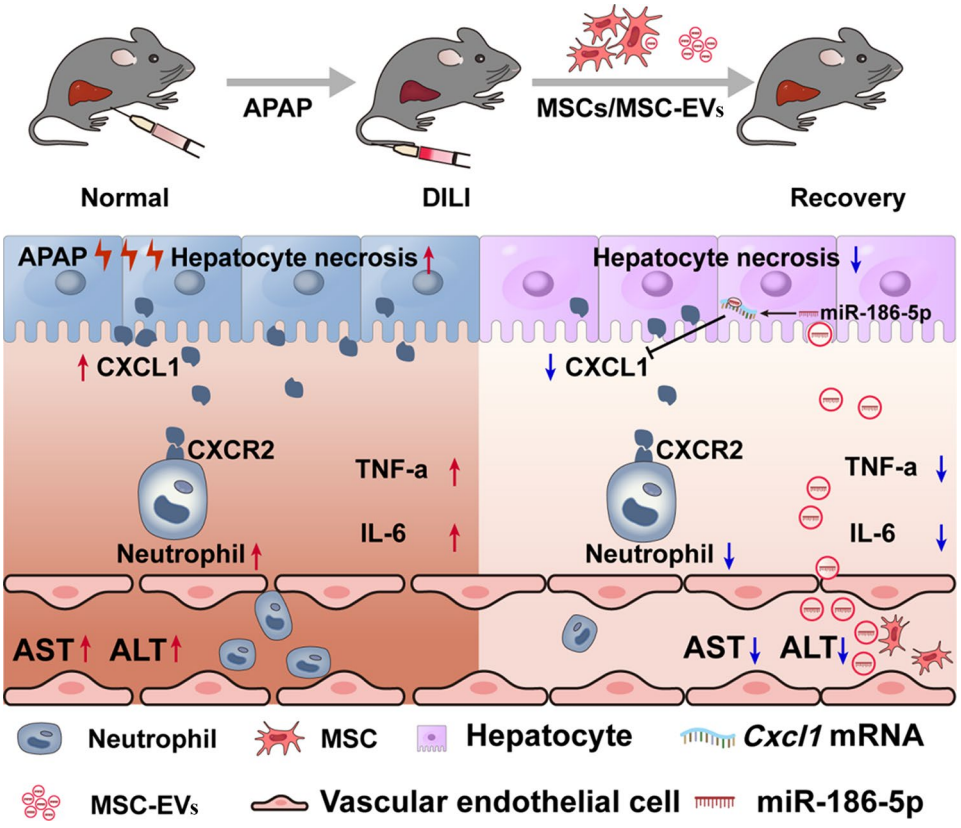

Keywords Mesenchymal stromal cells, Liver injury, Neutrophils, Extracellular vesicles, miR-186-5p, CXCL1

Introduction

Acetaminophen (APAP) is a commonly used antipyretic and analgesic drug in clinical practice, and APAP overdose is the most common cause of drug-induced acute liver injury (DILI) worldwide [1]. Approximately 50% of patients in the United States have acute liver failure (ALF) related to APAP-induced ALF [2, 3], and APAP-induced ALF is also considered a major public health problem in developing countries. At present, the only drug used for the early treatment of APAP overdose is the antioxidant N-acetylcysteine (NAC), which promotes the synthesis of glutathione (GSH) in the body to deplete N-acetyl-p-benzoquinone-imine (NAPQI), thereby reducing liver injury [4]. However, owing to the narrow treatment window, NAC is best used only within 8–10 h after APAP overdose, and a large proportion of patients miss the crucial window for NAC treatment. When patients progress to liver failure, the only effective treatment option is liver transplantation [5, 6]. Therefore, the exploration of more efficacious strategies to alleviate DILI has substantial clinical importance.

When APAP overdose occurs, the active metabolite NAPQI induces mitochondrial damage, causes hepatocyte necrosis, and activates the inflammatory response, which ultimately results in acute liver injury [7, 8]. In addition to APAP-induced hepatotoxicity, hepatocyte necrosis during DILI can further recruit neutrophils that activate the inflammatory response. Neutrophils are rapidly recruited to the injury site and mediate the intrahepatic inflammatory cascade [9]. Although, recent studies have shown that excessive neutrophil infiltration into the liver can cause severe inflammation and necrosis [10–12]. But, the specific regulatory network between the

hepatocyte damage and the inflammatory cascade during DILI remains unknown.

Mesenchymal stromal cells (MSCs) are adult stem cells that can be isolated from multiple human tissues, including bone marrow, gingiva, the umbilical cord (UC), and adipose tissue [13, 14]. They are the most frequently used cell type in stem cell therapy, offering a range of beneficial properties that contribute to regeneration, repair, and immune modulation. The therapeutic potential of MSCs has been demonstrated in the treatment of immune disorders [15, 16] and liver injury [17, 18]. Previous studies have reported that MSCs exert protective effects against APAP-induced liver damage via the secretion of multiple soluble paracrine factors, which inhibit inflammatory signaling pathways [19–22]. In addition, recent studies have demonstrated that extracellular vesicles (EVs), nanocarriers released by MSCs, play important roles in MSC therapy [23–26]. However, the specific regulatory mechanism of MSCs in the treatment of DILI is not fully understood.

In this study, we performed RNA transcriptomic analysis of liver tissues from mice with APAP-induced liver injury that were treated with or without MSCs. We found that MSCs improved liver function and ameliorated liver injury, and these effects were accompanied by decreased neutrophil infiltration. The RNA transcriptomic profiles revealed that MSCs modulated the inflammatory response in APAP-induced liver injury, and the overlap of the differentially expressed genes (DEGs) between the groups revealed that *Cxcl1*, which is a chemoattractant for neutrophils, was the only target gene. Mechanistically, via a luciferase reporter assay, we confirmed that MSC-EV-derived miR-186-5p bound to the 3'-UTR of *Cxcl1*to inhibit its expression in hepatocytes. Furthermore, neutralizing CXCL1 reduced drug-induced liver damage in vivo, and the agomir miR-186-5p showed excellent potential for treating APAP-induced ALF. Collectively, these results provide further insights into the targeted cellular and molecular mechanisms by which MSCs exert immunosuppressive effects in the treatment of DILI.

Materials and methods

Animals

Male C57BL/6 mice (8–10 w) were purchased from GemPharmatech (Guangdong, China) and were housed in a specific pathogen-free (SPF) barrier environment at the Sun Yat-sen University Laboratory Animal Centre (Guangdong, China).

APAP-induced liver injury mouse model

We prepared an APAP-induced liver injury model following previously published protocols [27]. Briefly, liver injury was induced by intraperitoneal injection of APAP (Rhawn, Shanghai, China) at a dose of 400 mg/kg. For MSC or MSC-EV transplantation, 1×10^6MSCs or 200 μg of MSC-EVs were suspended in 200 μL of ice-cold phosphate-buffered saline (PBS) and administered via tail vein injection 4 h after APAP administration. The control group was injected with PBS alone via the tail vein. At 24 h after APAP injection, the mice were anesthetized with sodium pentobarbital (100 mg/kg) for blood and liver tissue collection.

MSC isolation and identification

Human umbilical cords (UCs) were collected and processed after informed consent was provided by all the participants who were included in the study. Briefly, the UCs were dissected into 2 cm sections and the blood vessels were removed. The remaining tissue was then cut into smaller pieces and digested with collagenase IV for 1 h. The tissue was subsequently cultured in complete Dulbecco's modified Eagle's medium (DMEM), and the medium was changed every three days to remove nonadherent cells. MSCs exhibit fibroblast morphology and are characterized by a series of phenotypic markers and the ability to differentiate into trilineages. Passage 5 MSCs were used in all the experiments.

Flow cytometry

Flow cytometry was used to detect the phenotypic markers of MSCs, the proportion of neutrophils and the percentage of CD11b+F4/80+ cells in mouse livers and spleens. Mononuclear cells isolated from mouse liver and spleen tissues were stained with antibodies against CD11b, Ly6G and F4/80 from BioLegend (San Diego, USA). The fluorescence of the cells was subsequently detected via CytoFLEX (CytoFLEX LX, Beckman, USA). The antibodies and other reagents used are listed in Supplementary Table 1.

MSC-EV isolation and characterization

EVs were isolated according to methods described in previous studies. Briefly, we collected the supernatant of the MSCs, removed the cell fragments, and centrifuged them at 8600 g for 30 min. Finally, the EV precipitates were obtained by centrifuging at 23,700 rpm for 2.5 h with an ultrahigh-speed centrifuge (Optimal-90 K, Beckman, USA). We then used transmission electron microscopy (TEM) to identify the EVs (Tecnai T12, FEI, Czech Republic). The number and size of the isolated MSC-EVs (20 μl, 1:750 dilution with double-distilled water (ddH2O)) were detected via nanoparticle tracking analysis (NTA) (NanoSight NS300, Malvern, UK). The levels of the exosome protein markers Alix (CST, Massachusetts, USA), TSG101 (Abcam, Cambridge, UK) and CD63 (Abcam, Cambridge, UK) present in MSC-EVs were assessed in two samples of MSC-EVs and the corresponding MSCs via western blotting.

Measurements of aminotransferase (ALT) and aspartate transaminase (AST)

ALT and AST in the serum were measured via a Hitachi 7020 automatic biochemical analyzer (Hitachi, Tokyo, Japan).

Hematoxylin and eosin (H&E) staining and immunohistochemistry (IHC)

Liver paraffin sections (4 μm thick) were prepared for H&E and IHC staining. To block endogenous peroxidases, the sections were incubated in 3% hydrogen peroxide for 10 minutes. After antigen retrieval and Dako protein blocking (Dako), primary antibody incubation was performed, which included an anti-C-X-C motif chemokine 1 (CXCL1) polyclonal antibody (Proteintech, Rosemount, IL, USA), an anti-myeloperoxidase (MPO) monoclonal antibody (Proteintech, Rosemount, IL, USA), and a rabbit anti-Ly6G pAb (Servicebio, Wuhan, China); subsequently, the corresponding secondary antibodies were used. Following the final application of Diaminobenzidine (DAB) and hematoxylin staining, the samples were observed via an orthogonal fluorescence microscope (Nikon, USA), and images were acquired.

TUNEL staining

The TMR TUNEL Cell Apoptosis Detection Kit was obtained from Servicebio (Wuhan, China). The paraffin sections were pretreated with a gradient of xylene and ethanol, as recommended by the manufacturer. Afterward, these sections were incubated with a mixture of TdTase and fluorescein in the dark for one hour. The sections were subsequently immersed in Hoechst solution and incubated for eight minutes. Thereafter, the paraffin sections were photographed under a laser confocal microscope (STELLARIS STED, Leica, China).

Cell line and cell culture

AML12 cells were cultured in DMEM/Ham's F12 medium supplemented with 10% fetal bovine serum (FBS), 1% insulin-transferrin-selenium (ITS), and 1% penicillin and streptomycin. The cells were subcultured regularly via 0.25% trypsin and passaged at a 1:5 ratio every 3 days.

Western blotting analysis

Protein was extracted from cells, liver tissues, or MSC-EVs via RIPA buffer (Beyotime, Shanghai, China) supplemented with protease inhibitors (Roche, Indianapolis, IN, USA). Following the separation of protein lysates by 10% SDS–PAGE and their transfer onto polyvinylidene fluoride (PVDF) membranes, the membranes were blocked in TBST containing 5% BSA (MCE, New Jersey, USA) at room temperature for 1 h, followed by sequential incubation with appropriate primary and secondary antibodies. Western blotting results were obtained by scanning the protein bands via the Tanon 5200 Automated Chemiluminescent Image System (Tanon, Shanghai, China) with NcmECL Ultra chemiluminescence reagent (NCM, Suzhou, China). Supplementary Table 2shows the specific antibodies used for western blotting.

Enzyme-linked immunosorbent assay (ELISA)

First, the tissues were homogenized in 1 × PBS supplemented with protease inhibitors at a ratio of 1:9 (Roche, Indianapolis, IN, USA). ELISA were conducted following the manufacturer's protocol (CXCL1 ELISA kits from Elabscience, Wuhan, China). The absorption of the sample was recorded at 450 nm by a microplate reader (Thermo Scientific, Vantaa, Finland), and the concentrations of target proteins in the tissue homogenates were determined on the basis of the standard curve.

Anti-CXCL1 injections

Both the mCXCL1/KC mAb and the rIgG2A control were obtained from R&D Systems (Minneapolis, MN, USA). One hour before and 4 h after the intraperitoneal injection of APAP, 50 μg of mCXCL1/KC mAb or the rIgG2A control was intraperitoneally injected.

Transfection of mimics

AML12 cells were cultured in a 12-well plate at a density of 5×10^4cells per well. The miR-186-5p mimic (30 nM) or the same concentration of negative control (mimic NC) was subsequently transfected into these cells. RiboFECTTMCP reagent (RiboBio, Guangzhou, China) was simultaneously added to the medium to increase the transfection efficiency. The medium was changed 6 h later. In parallel, 5′FAM-labeled mimic-NC was transfected into AML12 cells with riboFECTTMCP reagent to determine the optimal transfection concentration via immunofluorescence. Twenty-four hours after transfection, the miRNA mimic transfection efficiency in AML12 cells was detected via RT−qPCR. The miR-186-5p mimic and negative control were acquired from RiboBio.

In vivo miRNA agomir treatment

To confirm the function of the miRNAs in vivo, an miRNA agomir (RiboBio, Guangzhou, China) was selected. After 4 h of APAP treatment, agomir-186-5p or the agomir-negative control (20 nmol; RiboBio) was administered via tail vein injection. All the injections were administered as described in previous studies [28, 29].

Dual-luciferase reporter assay

The pmirGLO luciferase vector was a kind gift from Professor Weicheng Liang. The Cxcl1 3'-UTR fragment was inserted into the pmirGLO luciferase vector

(pmirGLO-Cxcl1-WT). We subsequently constructed a mutant Cxcl1 plasmid (pmirGLO-Cxcl1-MUT) with a Mut Express Fast Mutagenesis Kit (Vazyme, Nanjing, China). After the appropriate plasmid (30 ng/well) was transfected into 293T cells for 48 h, luciferase assays were conducted with a Dual Luciferase Reporter Assay Kit (Vazyme, Nanjing, China), and the signal intensities of firefly luciferase and Renilla luciferase were measured with a microplate reader (INFINITE 200 PRO, Tecan, Switzerland). The transcriptional activity was assessed by normalizing the firefly luciferase activity to that of Renilla luciferase.

Isolation of neutrophils and migration assay

Neutrophils were isolated from mouse bone marrow via a Percoll density gradient as previously described [30]. Briefly, mouse bone marrow cells were suspended by flushing the femur and tibia with 1 × PBS, followed by filtration through a 100 μm mesh sieve. Neutrophils were isolated from mouse bone marrow via gradient centrifugation (2500 g, 30 min) with 62% Percoll and 81% Percoll at 4 °C. The neutrophils were subsequently stained with antibodies against CD11b (BioLegend, San Diego, USA) and Ly6G (BioLegend, San Diego, USA) to determine the purity of the isolated neutrophils.

Neutrophils were labeled with 5 μM CFSE (Invitrogen, California, USA) at 37 °C for 15 min. A neutrophil migration assay was subsequently performed according to previous methods [31]. A total of 1×10^5 neutrophils were placed in the upper chamber of a Transwell device (Corning, NY, USA), and 1×10^5 APAP-pretreated AML12 cells were seeded in the lower chamber. Following a 2 h incubation period, the number of neutrophils that had migrated was determined.

RNA isolation and real-time RT–qPCR

Total RNA was extracted from tissues or cells via a Fast Reverse Transcription Kit with gDNA remover (ESscience, Shanghai, China). Reverse transcription was conducted via an RNA Quick Purification Kit (ESscience, Shanghai, China). Reverse transcription of miRNA into cDNA was performed via the GoldenStartTM RT6 cDNA Synthesis Kit Ver.2 (Tsingke Biotech, Beijing, China). The internal control for miRNA was U6 RNA. 18 S or β-actin was used as the internal control for mRNA expression. Each sample was subjected to RT–qPCR on a Light Cycler 480 II (Roche, Indianapolis, IN, USA) with replicate wells using ChamQ SYBR RT–qPCR Master Mix (Vazyme, Nanjing, China). All primer sequences that were used for RT–qPCR are listed in Supplementary Table 3.

RNA sequencing and data processing

The samples were prepared, sequenced, and analyzed as previously reported [32]. Gene set enrichment analysis (GSEA) was performed with GSEA software (https://www.broadinstitute.org/gsea/). DEGs were identified and analyzed with DESeq2 on the basis of the following cutoff criteria: $p<0.05$ and $|Fc|>1.5$. The DEGs were subjected to GO and KEGG pathway analyses via the online Database for Annotation Visualization and Integrated Discovery (DAVID), with a statistical significance threshold of $p<0.05$. The sequencing data generated in this study have been submitted to the Gene Expression Omnibus (GEO) database with the accession number GSE252192.

Clinical data and specimen collection

All clinical procedures were approved by the Ethics Committee of the Third Affiliated Hospital of Sun Yat-sen University (Approval number: RG2023-301-02). Liver specimens were obtained from four patients who underwent transplantation with drug-induced liver failure. Healthy liver paraffin sections were obtained from the liver tissue surrounding the hemangioma in five hepatic hemangioma patients. All clinical samples were obtained at the Third Affiliated Hospital of Sun Yat-sen University with written informed consent from patients or their guardians. IHC analysis was used to determine CXCL1 and MPO expression in liver tissue sections.

Statistical analysis

All the results are expressed as the means ± SD. Student's t test and one-way ANOVA were used for statistical analyses between two groups or multigroup comparisons. Analysis and graphing were performed via GraphPad Prism version 9.0 (GraphPad 9.0, San Diego, CA, USA). $P<0.05$ was considered statistically significant. (ns: not significant; $^{*}P<0.05$; $^{**}P<0.01$; $^{***}P<0.001$; $^{****}P<0.0001$)

Checklist statement

The work has been reported in line with the ARRIVE guidelines 2.0.

Results

MSCs alleviate APAP-induced acute liver injury

To study the impact of MSCs on DILI, we prepared an animal model of liver injury via the intraperitoneal injection of 400 mg/kg APAP. The surface markers and differentiation capacities of the MSCs used in this study were assessed (Supplementary Fig. 1A–C). We performed MSC infusion and sample collection, as shown in Fig. 1A. The APAP group presented significant liver necrotic damage and high levels of AST and ALT, whereas the MSC group presented minimal liver necrotic damage and reduced levels of AST and ALT (Fig. 1B-D). TUNEL staining of liver sections revealed extensive apoptosis in liver tissues from the APAP group, whereas this effect was alleviated by MSC therapy (Supplementary Fig. 2A-B). Innate

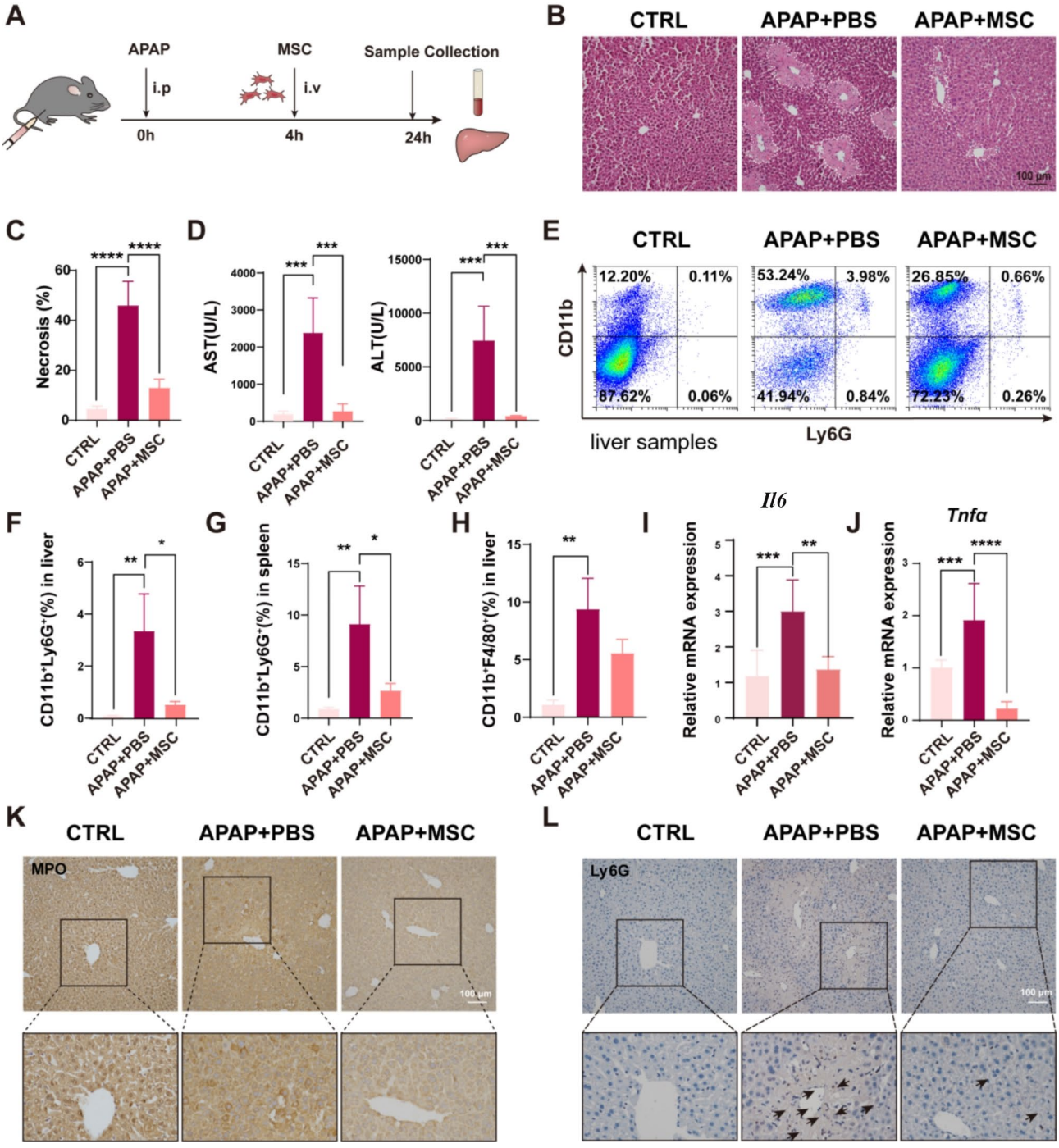

Fig. 1 MSCs attenuate APAP-induced acute liver injury. **A**) Schematic illustration of the experimental design. **B**) Representative images of HE-stained liver tissue from the indicated groups of mice. Scale bar = 100 μm. **C**) The percentage of the liver necrosis area ($n = 5$/group). **D**) Statistical graph of the serum AST and ALT levels in the indicated groups ($n = 5$/group). **E**) Representative dot plots of neutrophils ($CD11b^+Ly6G^+$) in mouse liver tissue detected by flow cytometry. **F**) Bar graph representing the statistical data in Fig. 1E ($n = 3$/group). **G**) Bar graph of neutrophils ($CD11b^+Ly6G^+$) in the mouse spleen detected by flow cytometry ($n = 3$/group). **H**) Bar graph of Kupffer cells ($CD11b^+F4/80^+$) in mouse livers detected by flow cytometry ($n = 3$/group). **I**) The mRNA expression levels of *Il6* in the liver tissues of the indicated groups of mice were detected via RT–qPCR ($n = 6$/group). **J**) The mRNA expression levels of *Tnfa* in the liver tissues of the indicated groups of mice were detected by RT–qPCR ($n = 8$/group). **K**) Representative images of MPO immunohistochemical staining of liver tissue from the indicated groups of mice. Scale bar = 100 μm. **L**) Representative images of Ly6G immunohistochemical staining of liver tissue from the indicated groups of mice. Scale bar = 100 μm

immune cells reportedly play major roles in liver injury [33]. The flow cytometry data revealed an increase in the percentage of neutrophils and Kupffer cells in both the liver and spleen after APAP treatment. In contrast, the administration of MSCs significantly attenuated neutrophil infiltration in both the liver and spleen but did not affect the percentage of Kupffer cells (Fig. 1E-H). Compared with APAP alone, MSCs significantly attenuated *Il6* and *Tnfα* mRNA expression in the liver (Fig. 1I and J). During immune responses, neutrophils release MPO to eliminate pathogens [34, 35]. Immunohistochemical staining revealed higher levels of Ly6G and MPO protein signals in the livers of APAP-treated mice than in those of control mice. The expression levels of MPO and Ly6G were decreased in the MSC group (Fig. 1K and L). These data demonstrate that MSCs can inhibit the infiltration of neutrophils into the liver and ameliorate APAP-induced liver injury.

Identification of Cxcl1 as a critical target gene of MSC treatment

Liver tissues from the control (CTRL) group, the APAP+PBS (APAP_PBS) group, and the APAP+MSC (APAP_MSC) group 24 h after APAP administration were subjected to RNA sequencing, with the aim of investigating potential target genes with altered expression following MSC treatment. A volcano plot was generated to visualize the DEGs between the CTRL and APAP_PBS groups and between the APAP_PBS and APAP_MSC groups (Fig. 2A). According to the KEGG pathway enrichment analysis, the DEGs were found to be associated primarily with the immune system (Fig. 2B and C). A Venn diagram was generated to analyze the DEGs between the CTRL group and the APAP_PBS group, as well as between the APAP group and the APAP_MSC group. The analysis revealed 206 DEGs between the CTRL and APAP_PBS groups that exhibited opposite expression trends compared with the DEGs between the APAP_PBS and APAP_MSC groups (Fig. 2D). The GSEA results revealed that neutrophil-related immune responses, including neutrophil migration, the TNF signaling pathway, leukocyte transendothelial migration, and the chemokine signaling pathway, were enriched in the APAP_PBS group and repressed in the APAP_MSC group (Fig. 2E and F, Supplementary Fig. 2C). The top 20 genes among the DEGs are presented in a heatmap (Fig. 2G). Among these genes, *Cxcl1*, which is a member of the CXC chemokine family, is closely related to immune system activation and serves as a chemoattractant for various immune cells, especially neutrophils. RT–qPCR and ELISA data confirmed that Cxcl1 expression in mouse livers was increased after APAP administration but was significantly decreased after MSC treatment (Fig. 2H and I). Furthermore, we detected a strong correlation between the *Cxcl1* mRNA level and the percentage of CD11b+Ly6G+ cells in the liver (Fig. 2J). Similarly, immunohistochemical staining revealed increased Cxcl1 protein signals in the APAP group, whereas the levels in the MSC-treated group were decreased (Fig. 2K). Finally, we detected increased expression of CXCL1 and MPO in liver tissues from DILI patients (Supplementary Fig. 2D and 2E), suggesting that CXCL1 is closely associated with DILI. Taken together, these results suggest that MSCs may inhibit neutrophil-mediated immune responses by targeting CXCL1.

CXCL1 is involved in the exacerbation of liver injury during APAP-induced ALF

To further examine the impact of CXCL1 on APAP-induced liver injury, we injected a CXCL1 neutralizing antibody into model mice 1 h before and 4 h after intraperitoneal APAP administration. In addition, a control group was established and received injections of an anti-IgG antibody. We collected peripheral blood and liver tissues for analysis 24 h after APAP administration (Fig. 3A). Compared with the IgG group, CXCL1 neutralization reduced the extent and necrosis area of liver injury, as well as ALT and AST levels (Fig. 3B-D). TUNEL staining also revealed that CXCL1 neutralization reduced the number of apoptotic cells in liver tissues (Supplementary Fig. 3A and 3B). Flow cytometry data revealed that CXCL1 neutralization reduced the percentage of neutrophils in both the liver and spleen but did not affect the percentage of Kupffer cells (Fig. 3E-G and Supplementary Fig. 3C). The RT–qPCR results revealed that neutralization of CXCL1 decreased the levels of *Cxcl1*, *Il6* and *Tnfα* in liver tissue (Fig. 3H–J). Immunohistochemical staining also revealed lower levels of the MPO, Ly6G and Cxcl1 proteins in the livers of the CXCL1 neutralization group (Supplementary Fig. 3D and Fig. 3K-L). Overall, these results indicate that CXCL1 exacerbates liver injury and promotes neutrophil infiltration after APAP administration.

MSC-EVs reduce hepatic damage and neutrophil infiltration in vivo

A previous study reported that intravenously injected MSCs that lodge in the lungs promptly undergo apoptosis and are cleared within 24 h [36]. EVs have unique biological functions and therapeutic potential similar to those of MSCs, as well as being a means of long-distance cell-to-cell communication in the body [37]. We therefore explored the therapeutic effectiveness of MSC-EVs in the treatment of DILI. EVs were obtained from the supernatant of MSCs via ultracentrifugation and characterized via transmission electron microscopy (TEM), nanoparticle tracking analysis (NTA) and western blotting (Supplementary Fig. 4A–C). The therapeutic transplantation

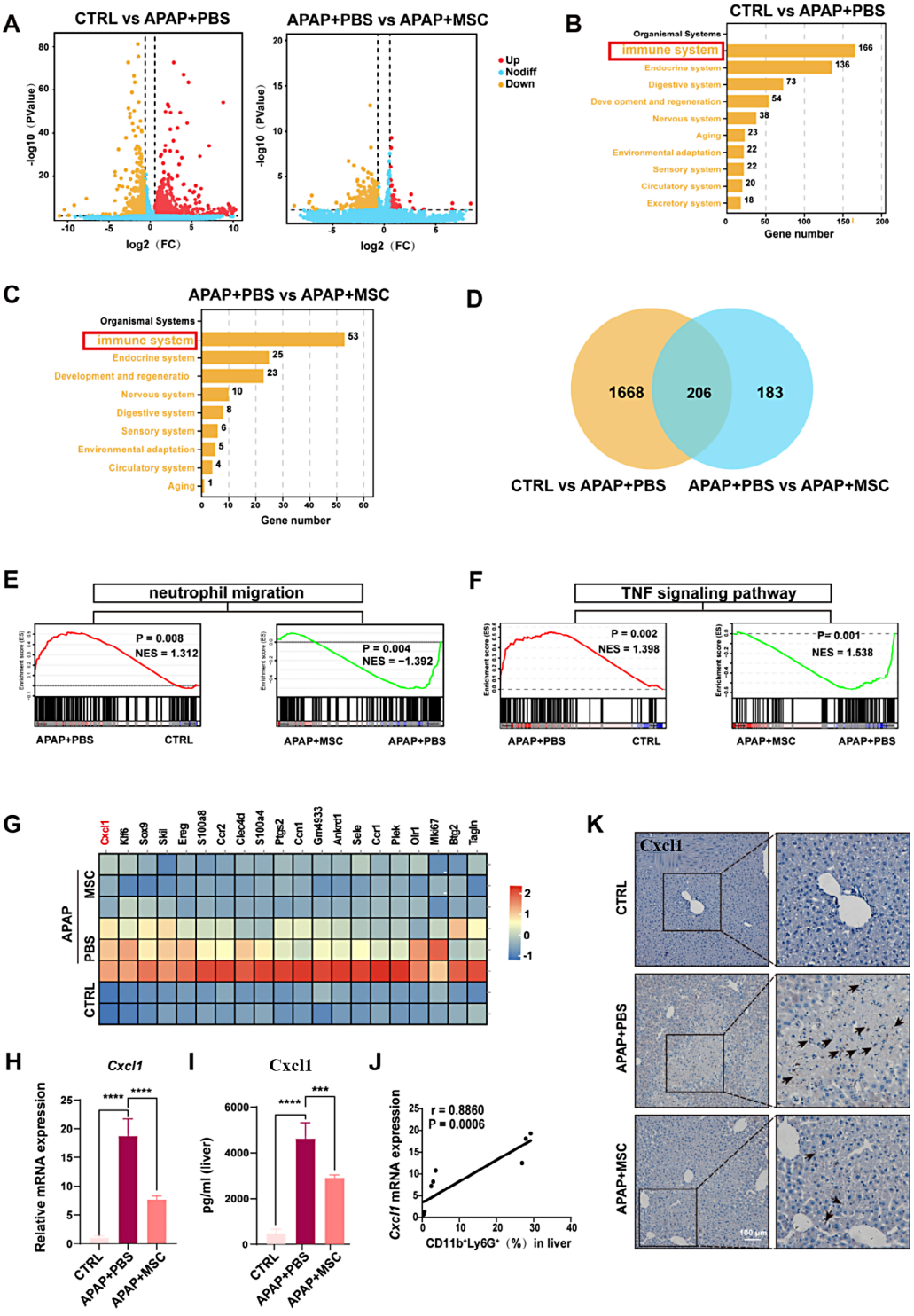

Fig. 2 Identification of Cxcl1 as a key target gene in MSC therapy. **A**) Volcano plot displaying the differentially expressed genes (DEGs) between the CTRL and APAP + PBS groups and between the APAP + PBS and APAP + MSC groups. **B**) Enriched pathways of organismal system classes for DEGs in the CTRL vs. APAP + PBS groups. **C**) Enriched pathways of organismal system classes for DEGs in the APAP + PBS vs. APAP + MSC groups. **D**) Venn diagram showing the intersection of DEGs between the CTRL and APAP + PBS groups and the APAP + PBS and APAP + MSC groups. **E**) Gene set enrichment analysis (GSEA) of neutrophil migration and **F**) the TNF signaling pathway. **G**) Heatmap displaying the top 20 genes with the highest expression levels among the DEGs at the intersection of the gene sets from Fig. 2D. **H**) The expression levels of *Cxcl1* mRNA in the liver tissue of the indicated groups of mice were detected via RT–qPCR ($n = 4$/group). **I**) The protein expression levels of Cxcl1 in liver tissue homogenates from the indicated groups of mice were detected via ELISA ($n = 5$/group). **J**) The correlation between hepatic *Cxcl1* mRNA expression and $CD11b^{+}Ly6G^{+}$ cells in liver tissue ($n = 16$). **K**) Representative images of Cxcl1 immunohistochemical staining of liver tissue from the indicated groups of mice. Scale bar = 100 μm

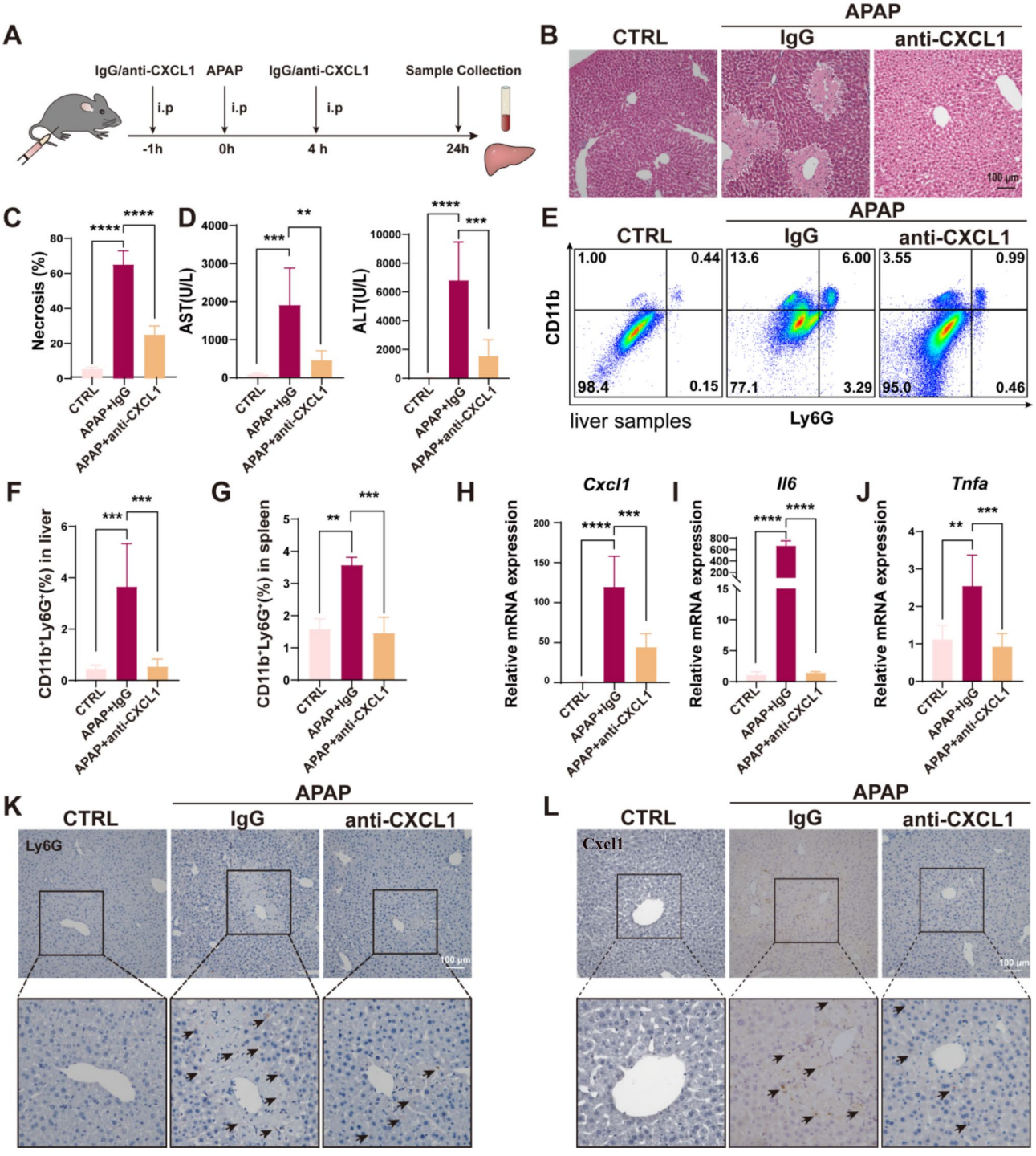

Fig. 3 CXCL1 is a key factor involved in the aggravation of liver injury in APAP-induced ALF. **A**) Schematic illustration of the experimental design. **B**) Representative images of HE-stained liver tissue from the indicated groups of mice. Scale bar = 100 μm. **C**) The percentage of the liver necrosis area ($n = 5$/group). **D**) Statistical graph of the serum AST and ALT levels in each group of mice ($n = 6$/group). **E**-**F**) Representative dot plots of neutrophils ($CD11b^+Ly6G^+$) in mouse liver tissue detected by flow cytometry and the corresponding statistical data. ($n = 5$/group). **G**) Bar graph of neutrophils ($CD11b^+Ly6G^+$) in the mouse spleen detected by flow cytometry ($n = 3$/group). **H**) The mRNA expression levels of *Cxcl1* in the liver tissue of the indicated groups of mice were detected by RT–qPCR ($n = 6$/group). **I**) The mRNA expression levels of *Il6* in the liver tissue of the indicated groups of mice were detected by RT–qPCR ($n = 4$/group). **J**) The mRNA expression levels of *Tnfa* in the liver tissue of the indicated groups of mice were detected by RT–qPCR ($n = 6$/group). **K**) Representative images of Ly6G immunohistochemical staining of liver tissue from the indicated groups of mice. Scale bar = 100 μm. **L**) Representative images of Cxcl1 immunohistochemical staining of liver tissue from the indicated groups of mice. Scale bar = 100 μm

procedures are illustrated in Fig. 4A. As expected, the livers of the mice in the MSC-EV-treated group presented smaller necrotic areas (Fig. 4B-C) and lower levels of serum transaminases (Fig. 4D). Flow cytometry analysis also revealed reduced neutrophil infiltration into both the liver and spleen after MSC-EV treatment (Fig. 4E-G). RT−qPCR analysis further confirmed the downregulation of *Cxcl1*, *Il6*, and *Tnfα* mRNA expression in mouse livers after EV treatment (Fig. 4H–J). Similarly, immunohistochemical staining revealed decreased protein expression of MPO, Ly6G and Cxcl1 in the livers of the mice after MSC-EV treatment (Supplementary Fig. 5A and Fig. 4K-L). Overall, these findings indicate that MSC-EVs exert significant therapeutic effects on APAP-induced liver injury in mice.

EVs derived from MSCs inhibit hepatocyte CXCL1 production in vitro

Next, to establish an in vitro model to examine EV target cells, we investigated the source of CXCL1 in the liver. During liver injury, hepatocytes and stromal cells in the liver have been shown in previous studies to produce CXCL1 [38]. We harvested primary hepatocytes (PHCs) and nonparenchymal cells (NPCs) from the livers of WT mice and APAP-treated mice. *Cxcl1* mRNA expression was greater in PHCs than in NPCs from the livers of APAP-treated WT mice (Supplementary Fig. 5B). We then treated AML12 cells, a mouse hepatocyte cell line, with APAP and added MSC-EVs to evaluate the degree of hepatocyte injury (Fig. 5A). An apoptosis assay revealed that MSC-EVs significantly decreased the number of apoptotic AML12 cells (Fig. 5B and C). Compared with those in APAP-treated AML12 cells, the mRNA expression levels of *Cxcl1* in APAP- and MSC-EV-treated AML12 cells were lower (Fig. 5D). In addition, we established a coculture system with hepatocytes and CFSE-labeled neutrophils (Fig. 5E). The number of neutrophils was confirmed to be >90% pure by flow cytometric analysis (Supplementary Fig. 5C), and the Transwell results revealed that APAP treatment induced neutrophil migration, which was inhibited by MSC-EVs (Fig. 5F). These findings indicate that MSC-EVs protect hepatocytes from APAP-induced damage by regulating CXCL1 expression.

miR-186-5p directly targets CXCL1 expression in hepatocytes

MicroRNAs (miRNAs) can modulate the expression of target genes that encode proteins by binding to the 3'-UTRs of their target genes [39]. EVs derived from MSCs contain abundant miRNAs, which are delivered to different tissues or cells to exert their biological effects [40]. We predicted potential miRNAs that could interact with Cxcl1 via bioinformatics websites (miRDB and ENCORI) and compared these results with existing MSC-EV miRNA sequencing data (GSE215041). The top hit was identified as miR-186-5p (Fig. 6A). Next, we identified putative binding sites for miR-186-5p within the 3'-UTRs of the human and mouse Cxcl1 mRNA sequences (Fig. 6B). To confirm these predictions, we constructed dual-luciferase reporter plasmids, namely, pmirGLO-Cxcl1-WT and pmirGLO-Cxcl1-MUT, and transfected them into 293T cells. After miR-186-5p stimulation, the luciferase activity of the WT sequence decreased, and this response was abolished by mutation of the 3'-UTR of Cxcl1 (Fig. 6C). To study the therapeutic effect of miR-186-5p on DILI in vitro, we synthesized a mimic of miR-186-5p. The synthetic mimic (mimic-miR-186-5p) and control mimic (mimic-NC) were transfected into AML12 cells. To determine the optimal concentration of mimic, we transfected the different concentrations with a 5'-FAM-labeled mimic NC and detected them by immunofluorescence (Supplementary Fig. 5D). The transfection efficiency of the miR-186-5p mimic was confirmed via RT−qPCR (Supplementary Fig. 5E). Compared with mimic-NC, the miR-186-5p mimic markedly reduced apoptosis in AML12 cells and increased the number of viable (Annexin V^-PI^-) AML12 cells after APAP treatment (Fig. 6D and E). In the hepatocyte and CFSE-labeled neutrophil coculture system (Fig. 6F), the Transwell assay results revealed that APAP treatment induced neutrophil migration in the mimic-NC group, but this migration was inhibited by the mimic-miR-186-5p (Fig. 6G). These results indicate that miR-186-5p inhibits the expression of CXCL1, thereby reducing the apoptosis of AML12 cells.

miR-186-5p alleviates APAP-induced liver injury

Encouraged by the hepatoprotective effect of miR-186-5p in vitro, we examined the therapeutic efficacy of miR-186-5p in an APAP-induced ALF model. The therapeutic transplantation procedures are illustrated in Fig. 7A. Compared with those in the negative control (agomir-NC) group, the apoptotic areas of the livers and the serum levels of transaminases in the agomir-186-5p group were lower (Fig. 7B-D). Flow cytometry analysis revealed that injection of agomir-186-5p significantly reduced neutrophil infiltration into liver and spleen tissues (Fig. 7E-G). Compared with those in the agomir-NC group, *Cxcl1*, *Il6*, and *Tnfα* mRNA expression levels were significantly lower in the agomir-186-5p group (Fig. 7H-J). Immunohistochemical staining revealed abundant MPO, Ly6G and Cxcl1 protein signals in liver sections from the agomir-NC group, whereas injection of agomir-186-5p significantly reduced the MPO, Ly6G and Cxcl1 protein signals (Supplementary Fig. 6A and Fig. 7K-L). Taken together, these findings indicate that MSC-EVs predominantly alleviate liver injury by delivering miR-186-5p and reducing neutrophil infiltration.

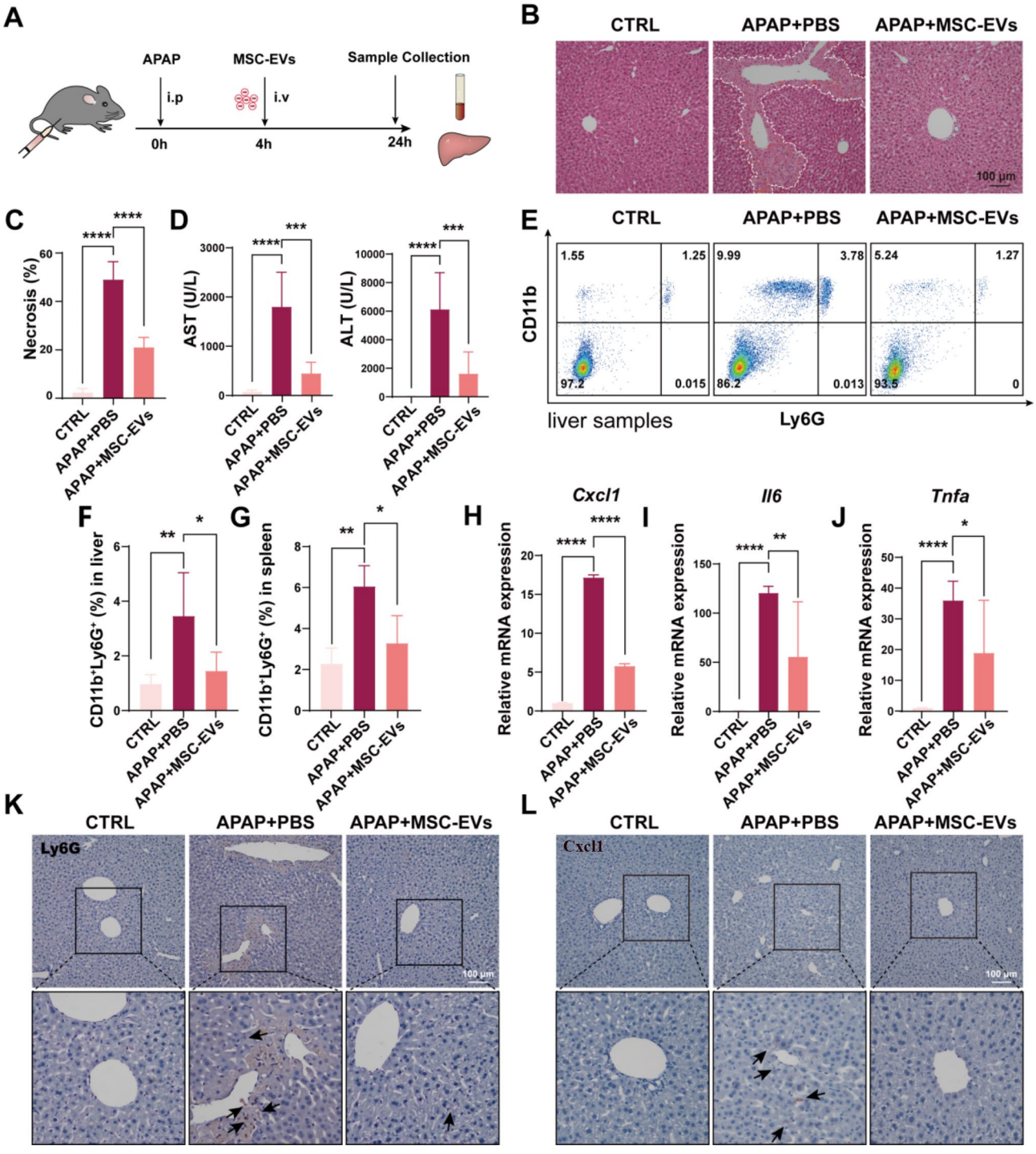

Fig. 4 MSC-EVs alleviate liver injury and neutrophil infiltration in vivo. **A**) Schematic illustration of the experimental design. **B**) Representative images of HE-stained liver tissue from the indicated groups of mice. Scale bar = 100 μm. **C**) The percentage of the liver necrosis area ($n = 5$/group). **D**) Statistical graph of the serum AST and ALT levels in the indicated groups ($n = 6$/group). **E**-**F**) Representative dot plots of neutrophils ($CD11b^+Ly6G^+$) in mouse liver tissue detected by flow cytometry and the corresponding statistical data ($n = 5$/group). **G**) Bar graph of neutrophils ($CD11b^+Ly6G^+$) in the mouse spleen detected by flow cytometry ($n = 3$/group). **H**) The mRNA expression levels of *Cxcl1* in the liver tissue of the indicated groups were detected by RT–qPCR ($n = 3$/group). **I**) The mRNA expression levels of *Il6* in the liver tissue of the indicated groups of mice were detected by RT–qPCR ($n = 6$/group). **J**) The mRNA expression levels of *Tnfa* in the liver tissue of the indicated groups of mice were detected by RT–qPCR ($n = 6$/group). **K**) Representative images of Ly6G immunohistochemical staining of liver tissue from the indicated groups (scale bar = 100 μm). **L**) Representative images of Cxcl1 immunohistochemical staining of liver tissue from the indicated groups of mice (scale bar = 100 μm)

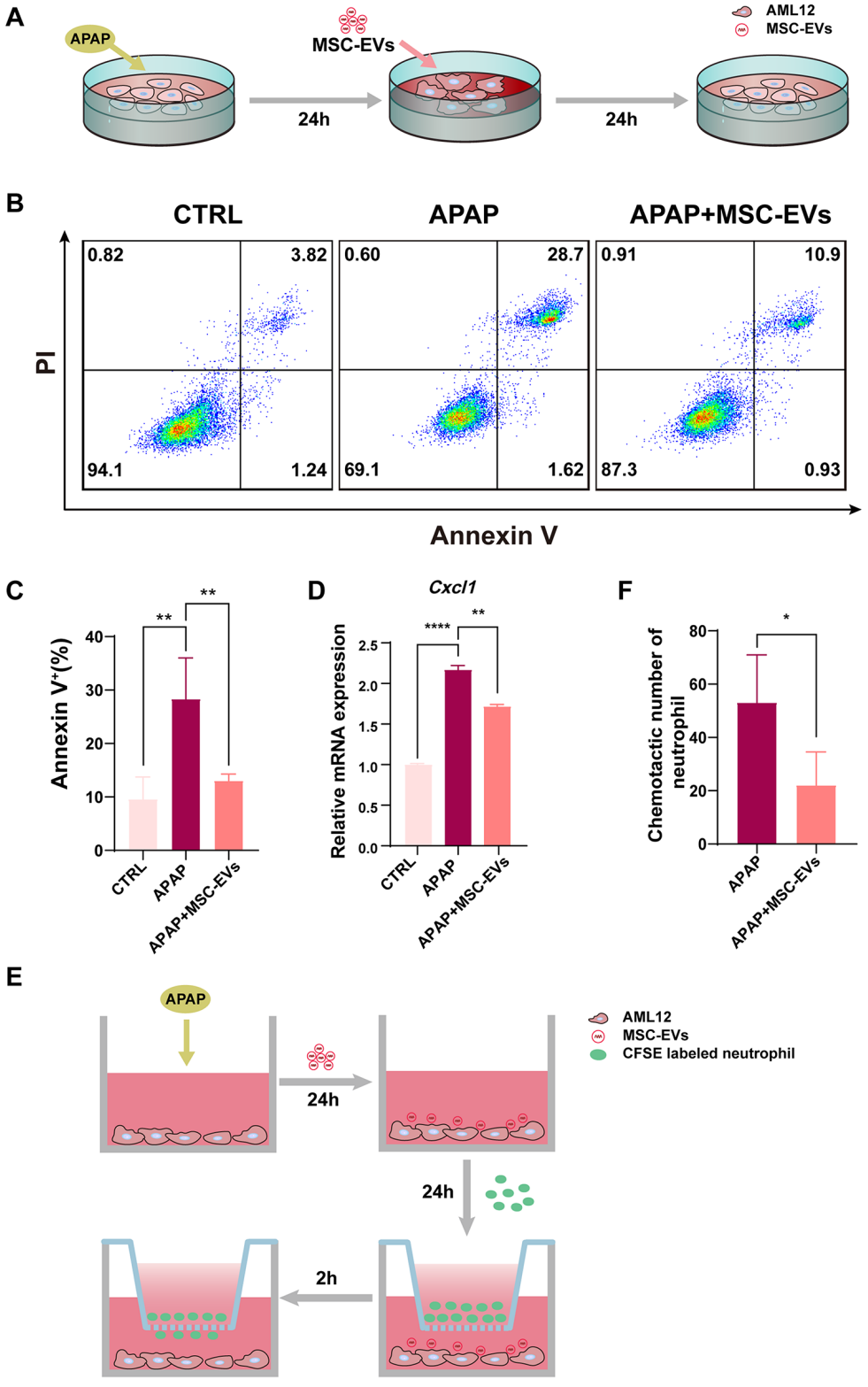

Fig. 5 MSC-EVs reduce hepatocyte apoptosis and neutrophil infiltration in vitro. **A**) Schematic illustration of the experimental design. **B**) Representative dot plots of Annexin V and PI staining of the indicated groups detected by flow cytometry. **C**) Bar graph showing the statistical data of the Annexin V$^+$ cells in Fig. 4B ($n = 4$/group). **D**) The mRNA expression levels of *Cxcl1* in the liver tissue of the indicated groups of mice were detected by RT–qPCR ($n = 3$/group). **E**) Schematic diagram of the neutrophil Transwell migration test for the APAP-induced AML12 cell injury model. **F**) Bar graph displaying the chemotactic number of CFSE-labeled neutrophils ($n = 5$/group)

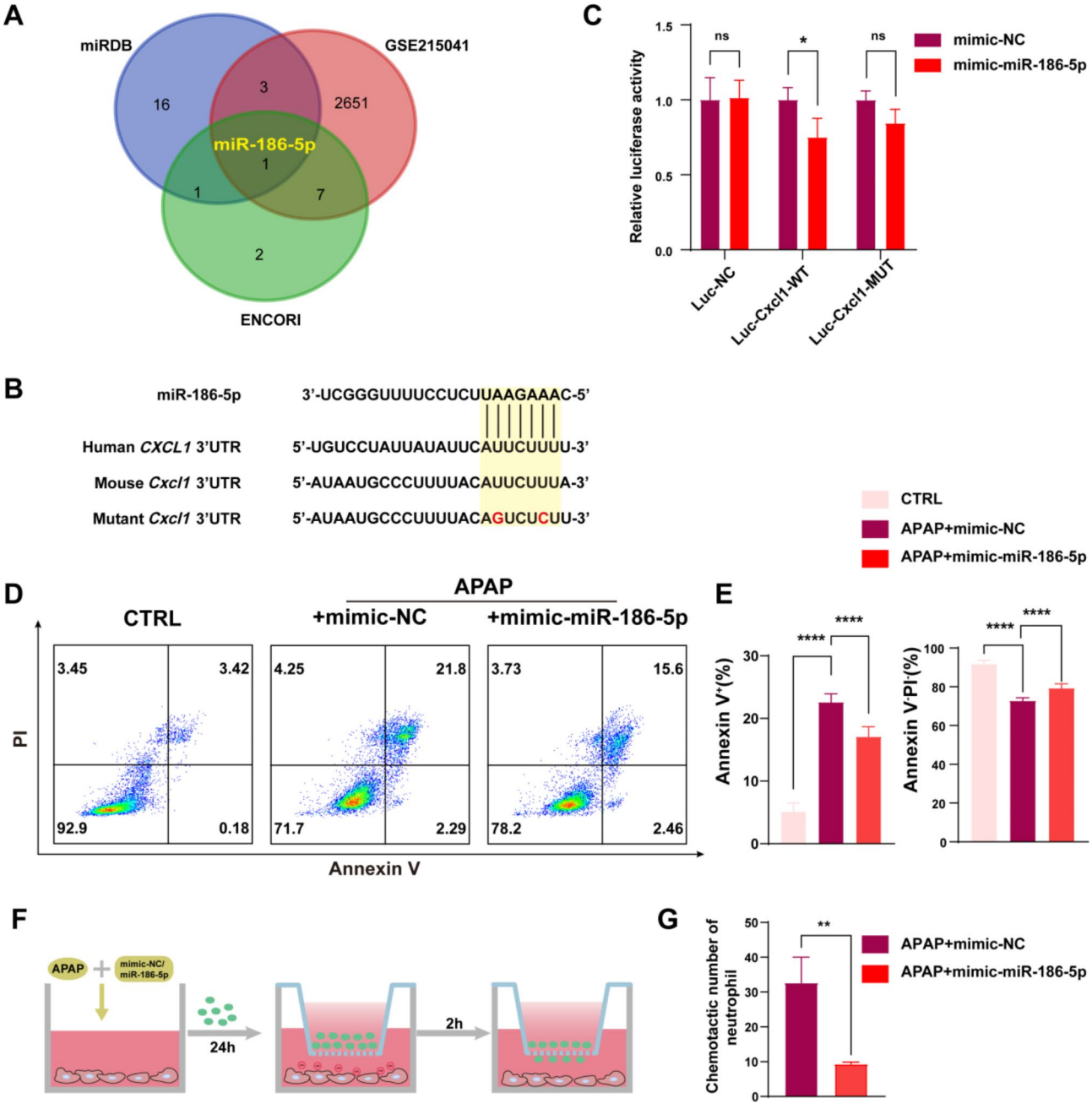

Fig. 6 miR-186-5p plays a key role in MSC-EV therapy for APAP-induced liver injury. **A**) Venn diagram showing the intersection between potential miRNAs predicted by bioinformatics websites to bind with Cxcl1 and the existing sequencing data. **B**) The potential binding site sequence of miR-186-5p and CXCL1. **C**) Bar graph representing the fluorescence intensity of HEK293T cells transfected with luciferase reporter plasmids determined via the Dual-Luciferase Reporter Assay System ($n=4$/group). **D**) Representative dot plots of Annexin V and PI staining of the indicated groups detected by flow cytometry. **E**) Bar graph showing the statistical data of the number of Annexin V^+ cells (left, $n=9$/group) and the number of Annexin V^-PI^- cells (right, $n=9$/group). **F**) Schematic diagram of the neutrophil Transwell migration test of miR-186-5p mimic transplantation for the treatment of the APAP-induced AML12 cell injury model. **G**) Bar graph displaying the chemotactic number of CFSE-labeled neutrophils ($n=3$/group)

Discussion

The objective of this study was to investigate the mechanism by which MSCs prevent the neutrophilic inflammatory response and protect against APAP-induced liver injury. To this end, we performed RNA transcriptomic analysis of liver tissues from mice with APAP-induced ALF that had been treated with or without MSCs. We found that MSC-derived miR-186-5p ameliorates acute liver injury by reducing CXCL1 production in hepatocytes, resulting in decreased neutrophil infiltration into the liver (Graphical abstract).

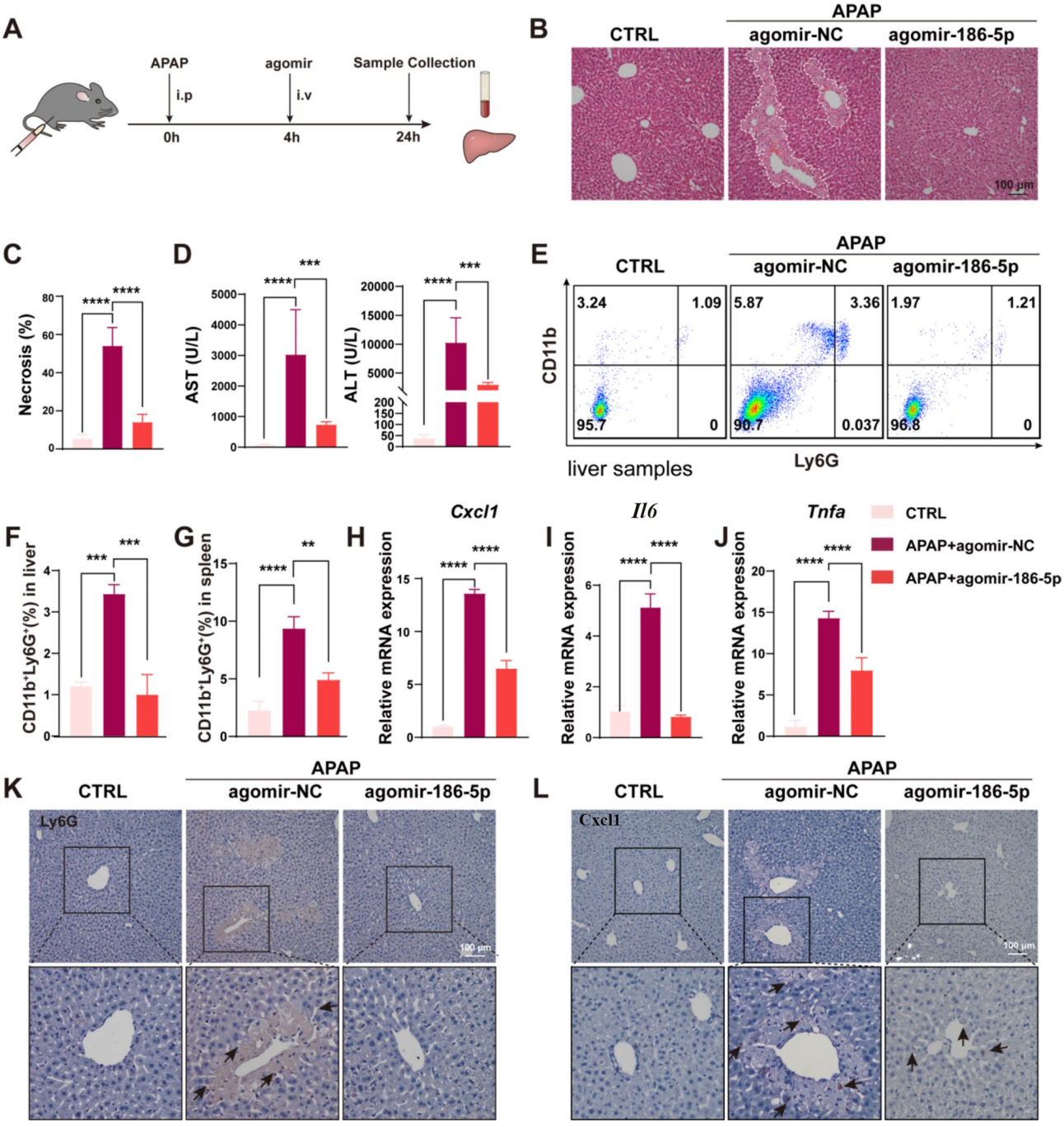

Fig. 7 Administration of the miR-186-5p agomir contributes to the amelioration of APAP-induced liver injury. **A**) Schematic illustration of the experimental design. **B**) Representative images of HE-stained liver tissue from the indicated groups of mice. Scale bar = 100 μm. **C**) The percentage of the liver necrosis area ($n = 5$/group). **D**) Statistical graph of the serum AST and ALT levels in the indicated groups of mice ($n = 6$/group). **E**) Representative dot plots of neutrophils ($CD11b^+Ly6G^+$) in mouse liver tissue detected by flow cytometry. **F**) Bar graph representing the statistical data in Fig. 7D ($n = 3$/group). **G**) Bar graph of neutrophils ($CD11b^+Ly6G^+$) in the mouse spleen detected by flow cytometry ($n = 3$/group). **H**) The mRNA expression levels of *Cxcl1* in the liver tissue of the indicated groups of mice were detected by RT–qPCR ($n = 4$/group). **I**) The mRNA expression levels of *Il6* in the liver tissue of the indicated groups of mice were detected by RT–qPCR ($n = 6$/group). **J**) The mRNA expression levels of *Tnfa* in the liver tissue of the indicated groups of mice were detected by RT–qPCR ($n = 6$/group). **K**) Representative images of Ly6G immunohistochemical staining of liver tissue from the indicated groups of mice. Scale bar = 100 μm. **L**) Representative images of Cxcl1 immunohistochemical staining of liver tissue from the indicated groups of mice. Scale bar = 100 μm

Neutrophils constitute the first line of defense in the innate immune response. It has also been suggested that, after APAP overdose, neutrophils cause liver impairment [41–43]. CXCL1 belongs to the subfamily of CXC chemokines [44], mediates neutrophil recruitment by binding to CXC chemokine receptor 2 (CXCR2) and plays an important role in neutrophil activation, recruitment, and infiltration [45]. In our studies, we verified that elevated CXCL1 expression was positively correlated with neutrophil infiltration in liver samples from both animals and patients with drug-induced ALF. CXCL1 could serve as a prognostic factor for patients who have developed ALI due to APAP, and it has been reported to be a prognostic factor for patients with hepatitis B virus-related acute–chronic liver failure [46]. A previous study demonstrated that CXCL1 contributes to the exacerbation of APAP-induced acute liver injury and recruits neutrophils to necrotic areas in the liver [38]. However, the source that produces CXCL1 during APAP-induced liver injury remains poorly understood. Through the isolation of primary hepatocytes and nonparenchymal cells, we found that CXCL1 was expressed predominantly by hepatocytes during APAP-induced liver injury. In another study, the expression of CXCL1 also increased in hepatocytes during Con A-induced acute liver injury [47]. This evidence may indicate that hepatocytes are the main source of CXCL1 during acute liver injury. Importantly, neutralization of CXCL1 ameliorated APAP-induced liver injury and decreased neutrophil infiltration. Our analyses highlights the role of CXCL1 in the chemotaxis of neutrophils during DILI, which may further contribute to the development of ALI.

Consistent with previous findings that MSCs possess anti- inflammatory and antioxidant functions to repair liver damage [21, 48–52], we found that MSC treatment alleviated DILI accompanied by decreased neutrophil infiltration. An analysis of the RNA-seq data revealed that Cxcl1 was markedly downregulated in the APAP+MSC group. The subsequent data revealed that increased CXCL1 expression and neutrophil infiltration were suppressed by MSC or MSC-EV treatment, which in turn reduced the subsequent activation of the immune cascade and the progression of hepatocyte apoptosis. Several miRNAs are associated with a reduction in CXCL1 expression through binding to its 3'-UTR [53–56]. To determine the possible role of miRNAs in MSC-EVs, we used an miRNA database (miRDB), which predicted a potential binding site of miR-186-5p in the 3'-UTR of mouse and human CXCL1 mRNAs. We further validated these findings with a luciferase reporter system. We observed that MSC-EVs or the miR-186-5p mimic protected AML12 cells against APAP-induced apoptosis, which is consistent with previous reports that MSC-EVs and miR-186-5p exert antioxidative stress and protective effects on cells [57–60]. These findings indicate that the regulation of CXCL1 expression in hepatocytes is essential for the ability of MSCs to mitigate DILI. However, whether other effects of MSCs, such as cell–cell contact or the secretion of soluble factors, play a role in regulating CXCL1 remains unknown and is an area for further research.

EVs contain a range of mRNAs and microRNAs that can be transferred to target cells in an endocrine or paracrine manner [61, 62]. MSC-EVs have the same therapeutic effect on liver injury [52, 63, 64] and have even better application prospects than cells because they have an extended circulation half-life and biocompatibility [65–67]. Our present study revealed that both MSCs and MSC-EVs have therapeutic effects on APAP-induced liver injury, but whether the effects of EVs are better than those of MSCs has not been determined, and the mechanism still needs further exploration.

Conclusion

In brief, the present study is the first to demonstrate that MSC-derived EVs deliver miR-186-5p to hepatocytes, downregulating CXCL1 expression and inhibiting neutrophil infiltration, thereby alleviating APAP-induced ALF. Our research elucidates the targeted cellular and molecular mechanisms by which MSC products exert immunosuppressive effects in the treatment of drug-induced liver failure.

Abbreviations

MSC-EVs	Mesenchymal stromal cell-derived extracellular vesicles
APAP	Acetaminophen
ALF	Acute liver failure
DILI	Drug-induced liver injury
AST	Aspartate transaminase
ALT	Alanine transaminase
NAC	N-acetylcysteine
NAPQI	N-acetyl-p-benzoquinone-imine
CXCL1	CXC motif chemokine 1
CXCR2	CXC chemokine receptor 2
MPO	Myeloperoxidase; IL-6:interleukin 6
TNF-α	Tumor necrosis factor
ELISA	Enzyme-linked immunosorbent assay
H&E	Hematoxylin and eosin
IHC	Immunohistochemistry
TUNEL	Terminal deoxynucleotidyl transferase (TdT) dUTP nick-end labeling
GSEA	Gene set enrichment analysis
PHC	Primary hepatocytes
NPC	Nonparenchymal cells; NC: negative control

Supplementary Information

The online version contains supplementary material available at https://doi.org/10.1186/s13287-024-03995-8.

Supplementary Material 1

Acknowledgements

This work was supported by the National Natural Science Foundation of China (81971526 and 82370629), the Science and Technology Program

of Guangzhou (202201020398, 202201020430), and the Natural Science Foundation of Guangdong Province (2022A1515012223). The authors declare that they have not used AI-generated work in this manuscript.

Author contributions
Erming Zhao: Conceptualization, methodology, writing - original draft, writing - review & editing, formal analysis. Rukang Liang: Methodology, writing - original draft, writing - review & editing. Panlong Li: Investigation, Methodology. Di Lu: Validation, Software, Formal analysis. Shuhan Chen: Investigation, Validation. Weikeng Tan: Validation, Software, Formal analysis. Yunfei Qin: Writing, review & editing, funding acquisition. Yana Zhang: Writing, review & editing. Yingcai Zhang: Writing - review & editing. Qi Zhang: Funding acquisition, project administration. Qiuli Liu: Conceptualization, Writing - original draft, Writing - review & editing, Funding acquisition, Supervision, Project administration.

Data availability
The data that support the findings of this study are available in the supplementary material of this article. All the fastq raw data files of the RNA-seq data generated in this study have been submitted to the Gene Expression Omnibus (GEO) database with the accession number GSE252192.

Declarations

Ethics approval and consent to participate
The animal protocol was reviewed and approved by the Institutional Animal Care and Use Committee (IACUC), Sun Yat-Sen University (Title: Mesenchymal stem cells alleviate acute liver injury in a mouse model induced by acetaminophen; Approval number: SYSU-IACUC-2023-000849; Date: May 25, 2023). For the patients' samples, the patients or their guardians provided written informed consent for participation in the study and the use of samples. All the human tissue experiments were approved by the Ethics Committee of the Third Affiliated Hospital of Sun Yat-sen University (Title: Role of the RNA-Editing Enzyme ADAR1 in Regulating the Immunosuppressive Function of Mesenchymal Stem Cells in the Treatment of Acute Liver Failure; Approval number: RG2023-301-02; Date: January 5, 2024).

Material availability
The materials used in this study are available in the supplementary material.

Conflict of interest
The authors declare that they have no conflicts of interest.

Author details
[1]Biotherapy Center, The Third Affiliated Hospital, Sun Yat-sen University, Guangzhou 510630, China
[2]Department of Otolaryngology-Head and Neck Surgery, The Third Affiliated Hospital of Sun Yat-Sen University, Guangzhou 510630, China
[3]Department of Allergy, The Third Affiliated Hospital of Sun Yat-Sen University, Guangzhou 510630, China
[4]Department of Hepatic Surgery and Liver Transplantation Centre, The Third Affiliated Hospital, Sun Yat-sen University, Guangzhou 510630, China

Received: 18 August 2024 / Accepted: 13 October 2024
Published online: 03 November 2024

References

1. Lee WM. Acetaminophen toxicity: changing perceptions on a social/medical issue. Hepatology. 2007;46:966–70.
2. Chayanupatkul M, Schiano TD. Acute Liver failure secondary to Drug-Induced Liver Injury. Clin Liver Dis. 2020;24:75–87.
3. Goldberg DS, Forde KA, Carbonari DM, Lewis JD, Leidl KB, Reddy KR, et al. Population-representative incidence of drug-induced acute liver failure based on an analysis of an integrated health care system. Gastroenterology. 2015;148:1353–61.
4. Bryan A, Pingali P, Faber A, Landry J, Akakpo JY, Jaeschke H, et al. High-dose acetaminophen with concurrent CYP2E1 inhibition has profound anticancer activity without liver toxicity. J Pharmacol Exp Ther. 2024;388:209–17.
5. Lee WM. Acetaminophen (APAP) hepatotoxicity-Isn't it time for APAP to go away? J Hepatol. 2017;67:1324–31.
6. Stravitz RT, Fontana RJ, Karvellas C, Durkalski V, McGuire B, Rule JA, et al. Future directions in acute liver failure. Hepatology. 2023;78:1266–89.
7. Kaplowitz N. Acetaminophen hepatoxicity: what do we know, what don't we know, and what do we do next? Hepatology. 2004;40:23–6.
8. Cai X, Cai H, Wang J, Yang Q, Guan J, Deng J, et al. Molecular pathogenesis of acetaminophen-induced liver injury and its treatment options. J Zhejiang Univ-Sc B. 2022;23:265–85.
9. Liu K, Wang FS, Xu R. Neutrophils in liver diseases: pathogenesis and therapeutic targets. Cell Mol Immunol. 2021;18:38–44.
10. Lawson JA, Farhood A, Hopper RD, Bajt ML, Jaeschke H. The hepatic inflammatory response after acetaminophen overdose: role of neutrophils. Toxicol Sci. 2000;54:509–16.
11. Wu W, Sun S, Wang Y, Zhao R, Ren H, Li Z, et al. Circulating Neutrophil Dysfunction in HBV-Related Acute-on-chronic liver failure. Front Immunol. 2021;12:620365.
12. Taylor NJ, Nishtala A, Manakkat VG, Abeles RD, Auzinger G, Bernal W, et al. Circulating neutrophil dysfunction in acute liver failure. Hepatology. 2013;57:1142–52.
13. Midha S, Jain KG, Bhaskar N, Kaur A, Rawat S, Giri S, et al. Tissue-specific mesenchymal stem cell-dependent osteogenesis in highly porous chitosan-based bone analogs. Stem Cell Transl Med. 2021;10:303–19.
14. Väänänen HK. Mesenchymal stem cells. Ann Med. 2005;37:469–79.
15. Wu X, Jiang J, Gu Z, Zhang J, Chen Y, Liu X. Mesenchymal stromal cell therapies: immunomodulatory properties and clinical progress. Stem Cell Res Ther. 2020;11:345.
16. Andrzejewska A, Lukomska B, Janowski M. Concise Review: mesenchymal stem cells: from roots to Boost. Stem Cells. 2019;37:855–64.
17. Liu P, Yao L, Hu X, Wang Z, Xiong Z, Jiang Y. Recent advances in the immunomodulation mechanism of mesenchymal stem cell therapy in liver diseases. J Gastroen Hepatol. 2023;38:1099–106.
18. Zhou J, Feng X, Zhu J, Feng B, Yao Q, Pan Q, et al. Mesenchymal stem cell treatment restores liver macrophages homeostasis to alleviate mouse acute liver injury revealed by single-cell analysis. Pharmacol Res. 2022;179:106229.
19. Yu M, Zhou M, Li J, Zong R, Yan Y, Kong L, et al. Notch-activated mesenchymal stromal/stem cells enhance the protective effect against acetaminophen-induced acute liver injury by activating AMPK/SIRT1 pathway. Stem Cell Res Ther. 2022;13:318.
20. Wang P, Cui Y, Wang J, Liu D, Tian Y, Liu K, et al. Mesenchymal stem cells protect against acetaminophen hepatotoxicity by secreting regenerative cytokine hepatocyte growth factor. Stem Cell Res Ther. 2022;13:94.
21. Cen Y, Lou G, Qi J, Li M, Zheng M, Liu Y. Adipose-Derived Mesenchymal Stem Cells Inhibit JNK-Mediated Mitochondrial Retrograde Pathway to Alleviate Acetaminophen-Induced Liver Injury. Antioxidants-Basel. 2023;12.
22. Liu Z, Meng F, Li C, Zhou X, Zeng X, He Y, et al. Human umbilical cord mesenchymal stromal cells rescue mice from acetaminophen-induced acute liver failure. Cytotherapy. 2014;16:1207–19.
23. Sitbon A, Delmotte PR, Goumard C, Turco C, Gautheron J, Conti F, et al. Therapeutic potentials of mesenchymal stromal cells-derived extracellular vesicles in liver failure and marginal liver graft rehabilitation: a scoping review. Minerva Anestesiol. 2023;89:690–706.
24. Gupta S, Pinky, Vishal, Sharma H, Soni N, Rao EP, et al. Comparative evaluation of Anti-fibrotic Effect of tissue specific mesenchymal stem cells derived Extracellular vesicles for the amelioration of CCl4 Induced Chronic Liver Injury. Stem Cell Rev Rep. 2022;18:1097–112.
25. Mardpour S, Ghanian MH, Sadeghi-Abandansari H, Mardpour S, Nazari A, Shekari F, et al. Hydrogel-mediated sustained systemic delivery of mesenchymal stem cell-derived extracellular vesicles improves hepatic regeneration in Chronic Liver failure. Acs Appl Mater Inter. 2019;11:37421–33.
26. Varderidou-Minasian S, Lorenowicz MJ. Mesenchymal stromal/stem cell-derived extracellular vesicles in tissue repair: challenges and opportunities. Theranostics. 2020;10:5979–97.
27. Gonther S, Bachmann M, Goren I, Huard A, Weigert A, Köhl J, et al. 3'mRNA sequencing reveals pro-regenerative properties of c5ar1 during resolution of murine acetaminophen-induced liver injury. Npj Regen Med. 2022;7:10.
28. Yang M, Du B, Xu L, Wang H, Wang Y, Lin K, et al. Glutamate-GABA imbalance mediated by mir-8-5p and its STTM regulates phase-related behavior of locusts. P Natl Acad Sci Usa. 2023;120:e2079307176.
29. Yang M, Wei Y, Jiang F, Wang Y, Guo X, He J, et al. MicroRNA-133 inhibits behavioral aggregation by controlling dopamine synthesis in locusts. Plos Genet. 2014;10:e1004206.

30. Liu L, Das S, Losert W, Parent CA. mTORC2 regulates neutrophil chemotaxis in a cAMP- and RhoA-dependent fashion. Dev Cell. 2010;19:845–57.
31. Wang T, Zhou Y, Zhou Z, Zhang P, Yan R, Sun L, et al. Secreted protease PRSS35 suppresses hepatocellular carcinoma by disabling CXCL2-mediated neutrophil extracellular traps. Nat Commun. 2023;14:1513.
32. Pan L, Liu C, Liu Q, Li Y, Du C, Kang X, et al. Human Wharton's jelly-derived mesenchymal stem cells alleviate concanavalin A-induced fulminant hepatitis by repressing NF-κB signaling and glycolysis. Stem Cell Res Ther. 2021;12:496.
33. Dong Z, Wei H, Sun R, Tian Z. The roles of innate immune cells in liver injury and regeneration. Cell Mol Immunol. 2007;4:241–52.
34. Pulli B, Ali M, Iwamoto Y, Zeller MW, Schob S, Linnoila JJ, et al. Myeloperoxidase-hepatocyte-stellate Cell Cross Talk promotes hepatocyte Injury and Fibrosis in Experimental Nonalcoholic Steatohepatitis. Antioxid Redox Sign. 2015;23:1255–69.
35. Rensen SS, Slaats Y, Nijhuis J, Jans A, Bieghs V, Driessen A, et al. Increased hepatic myeloperoxidase activity in obese subjects with nonalcoholic steatohepatitis. Am J Pathol. 2009;175:1473–82.
36. Pang S, D'Rozario J, Mendonca S, Bhuvan T, Payne NL, Zheng D, et al. Mesenchymal stromal cell apoptosis is required for their therapeutic function. Nat Commun. 2021;12:6495.
37. Lai P, Weng J, Guo L, Chen X, Du X. Novel insights into MSC-EVs therapy for immune diseases. Biomark Res. 2019;7:6.
38. Chang B, Xu MJ, Zhou Z, Cai Y, Li M, Wang W, et al. Short- or long-term high-fat diet feeding plus acute ethanol binge synergistically induce acute liver injury in mice: an important role for CXCL1. Hepatology. 2015;62:1070–85.
39. Gulyaeva LF, Kushlinskiy NE. Regulatory mechanisms of microRNA expression. J Transl Med. 2016;14:143.
40. Asgarpour K, Shojaei Z, Amiri F, Ai J, Mahjoubin-Tehran M, Ghasemi F, et al. Exosomal microRNAs derived from mesenchymal stem cells: cell-to-cell messages. Cell Commun Signal. 2020;18:149.
41. Liu ZX, Han D, Gunawan B, Kaplowitz N. Neutrophil depletion protects against murine acetaminophen hepatotoxicity. Hepatology. 2006;43:1220–30.
42. Jaeschke H, Liu J. Neutrophil depletion protects against murine acetaminophen hepatotoxicity: another perspective. Hepatology. 2007;45:1588–9.
43. Marques PE, Amaral SS, Pires DA, Nogueira LL, Soriani FM, Lima BH, et al. Chemokines and mitochondrial products activate neutrophils to amplify organ injury during mouse acute liver failure. Hepatology. 2012;56:1971–82.
44. Korbecki J, Barczak K, Gutowska I, Chlubek D, Baranowska-Bosiacka I. CXCL1: Gene, promoter, regulation of expression, mRNA Stability, Regulation of activity in the Intercellular Space. Int J Mol Sci. 2022;23.
45. Wu MM, Yang YC, Cai YX, Jiang S, Xiao H, Miao C, et al. Anti-CTLA-4 m2a antibody exacerbates Cardiac Injury in experimental autoimmune myocarditis mice by promoting Ccl5-Neutrophil infiltration. Adv Sci. 2024;11:e2400486.
46. Xiao L, Tang S, Zhang L, Ma S, Zhao Y, Zhang F, et al. Serum CXCL1 is a prognostic factor for patients with Hepatitis B Virus-related Acute-On-Chronic Liver failure. Front Med-Lausanne. 2021;8:657076.
47. Matsuo S, Nabekura T, Matsuda K, Shibuya K, Shibuya A. DNAM-1 Immunoreceptor protects mice from Concanavalin A-Induced Acute Liver Injury by reducing Neutrophil Infiltration. J Immunol. 2023;211:954–63.
48. Zhou J, Shi Y. Mesenchymal stem/stromal cells (MSCs): origin, immune regulation, and clinical applications. Cell Mol Immunol. 2023;20:555–7.
49. Shi Y, Hu G, Su J, Li W, Chen Q, Shou P, et al. Mesenchymal stem cells: a new strategy for immunosuppression and tissue repair. Cell Res. 2010;20:510–8.
50. Han Y, Yang J, Fang J, Zhou Y, Candi E, Wang J, et al. The secretion profile of mesenchymal stem cells and potential applications in treating human diseases. Signal Transduct Tar. 2022;7:92.
51. Fu X, Liu G, Halim A, Ju Y, Luo Q, Song AG. Mesenchymal Stem Cell Migration and Tissue Repair. Cells-Basel. 2019;8.
52. Huang YL, De Gregorio C, Silva V, Elorza ÁA, Léniz P, Aliaga-Tobar V et al. Administration of Secretome Derived from Human mesenchymal stem cells induces Hepatoprotective effects in models of Idiosyncratic Drug-Induced Liver Injury caused by amiodarone or tamoxifen. Cells-Basel. 2023;12.
53. Pecot CV, Rupaimoole R, Yang D, Akbani R, Ivan C, Lu C, et al. Tumour angiogenesis regulation by the miR-200 family. Nat Commun. 2013;4:2427.
54. Du Z, Wu T, Liu L, Luo B, Wei C. Extracellular vesicles-derived mir-150-5p secreted by adipose-derived mesenchymal stem cells inhibits CXCL1 expression to attenuate hepatic fibrosis. J Cell Mol Med. 2021;25:701–15.
55. Shrestha S, Yang CD, Hong HC, Chou CH, Tai CS, Chiew MY et al. Integrated MicroRNA-mRNA analysis reveals miR-204 inhibits cell proliferation in gastric Cancer by targeting CKS1B, CXCL1 and GPRC5A. Int J Mol Sci. 2017;19.
56. Liu CH, Jing XN, Liu XL, Qin SY, Liu MW, Hou CH. Tumor-suppressor miRNA-27b-5p regulates the growth and metastatic behaviors of ovarian carcinoma cells by targeting CXCL1. J Ovarian Res. 2020;13:92.
57. Yin S, Zhou Z, Fu P, Jin C, Wu P, Ji C, et al. Roles of extracellular vesicles in ageing-related chronic kidney disease: demon or angel. Pharmacol Res. 2023;193:106795.
58. Chen F, Li X, Li Z, Qiang Z, Ma H. Altered expression of MiR-186-5p and its target genes after spinal cord ischemia-reperfusion injury in rats. Neurosci Lett. 2020;718:134669.
59. Feng H, Zhang Z, Qing X, French SW, Liu D. Mir-186-5p promotes cell growth, migration and invasion of lung adenocarcinoma by targeting PTEN. Exp Mol Pathol. 2019;108:105–13.
60. Yang Y, Wang J, Zhang Y, Hu X, Li L, Chen P. Exosomes derived from mesenchymal stem cells ameliorate renal fibrosis via delivery of miR-186-5p. Hum Cell. 2022;35:83–97.
61. Si L, Bai J, Fu H, Qiu H, Guo R. The functions and potential roles of extracellular vesicle noncoding RNAs in gynecological malignancies. Cell Death Discov. 2021;7:258.
62. Colombo M, Raposo G, Théry C. Biogenesis, secretion, and intercellular interactions of exosomes and other extracellular vesicles. Annu Rev Cell Dev Bi. 2014;30:255–89.
63. Shokravi S, Borisov V, Zaman BA, Niazvand F, Hazrati R, Khah MM, et al. Mesenchymal stromal cells (MSCs) and their exosome in acute liver failure (ALF): a comprehensive review. Stem Cell Res Ther. 2022;13:192.
64. Yang F, Wu Y, Chen Y, Xi J, Chu Y, Jin J, et al. Human umbilical cord mesenchymal stem cell-derived exosomes ameliorate liver steatosis by promoting fatty acid oxidation and reducing fatty acid synthesis. Jhep Rep. 2023;5:100746.
65. Pirisinu M, Pham TC, Zhang DX, Hong TN, Nguyen LT, Le MT. Extracellular vesicles as natural therapeutic agents and innate drug delivery systems for cancer treatment: recent advances, current obstacles, and challenges for clinical translation. Semin Cancer Biol. 2022;80:340–55.
66. El AS, Lakhal S, Mäger I, Wood MJ. Exosomes for targeted siRNA delivery across biological barriers. Adv Drug Deliver Rev. 2013;65:391–7.
67. van Niel G, D'Angelo G, Raposo G. Shedding light on the cell biology of extracellular vesicles. Nat Rev Mol Cell Bio. 2018;19:213–28.

Publisher's note